

Landslide susceptibility deterministic approach using geographic information systems: application to Breaza town, Romania

Iuliana Armaş · Florin Vartolomei · Florica Stroia · Livioara Braşoveanu

Received: 26 December 2010 / Accepted: 4 September 2013 / Published online: 26 September 2013
© Springer Science+Business Media Dordrecht 2013

Abstract The study is a deterministic-based approach on landslide susceptibility. The purpose of the paper is to create quantitative susceptibility maps by joining the one-dimension infinite slope stability model with a raster-based GIS (ILWIS) and taking into account the spatial distribution of input parameters. A landslide-prone area, with relative homogeneous geology and geomorphology, located in the Subcarpathian sector of the Prahova River, Romania, was selected for the study. There are frequent problems caused by active landslides in the studied area, especially in years with heavy precipitation, often causing destruction of houses and roads situated on the slopes (1992, 1997, and 2005). Detailed surveys covering a 7-year period provided the necessary input data on slope parameters, hydrological components, and the geotechnical background. Two simulations were used: one on dry soil conditions and one on fully saturated soil conditions. A third test was based on the level of the groundwater table mapped in summer 2008. Detailed analyses were particularly focused on landslides to compare predicted results with actual results using field measurements. The model is very suitable for use in raster GIS because it can calculate slope instability on a pixel basis, each raster cell being considered individually. The drawback of the model is the highly detailed data of input parameters. Despite this disadvantage, in conclusion, the usefulness of slope stability models on a large-scale basis was emphasized under infinitely high failure plain conditions and lithological homogeneity.

Keywords Shallow landslides · Infinite slope stability model · Landslide susceptibility · GIS

I. Armaş (✉) · F. Stroia · L. Braşoveanu
University of Bucharest, Bucharest, Romania
e-mail: iulia_armas@geo.unibuc.ro

F. Vartolomei
Spiru Haret University, Bucharest, Romania

1 Introduction

Within the slope processes, landslides have the biggest impact on human communities (e.g., Schuster 1995a, b; Schuster and Fleming 1986; Alexander 1991, 1992; US Geological Survey 1997). Hazards and risks caused by slope instabilities, especially in hilly and mountainous areas, have a primary importance in geomorphology research, especially after 1990 due to an explosive increase in the value of damages and implicit to this, insurance claims due to active landslides disasters (UN/ISDR 2004; EM-DAT 2006).

Various methods of active landslide susceptibility mapping were developed and a vast literature in the field already exists. Within the analysis of slope instabilities, review of the scientific literature shows four main methods: inventory, heuristic, statistical, and deterministic (e.g., Montgomery and Dietrich 1994; Hoek and Bray 1997; Soeters and van Westen 1996; van Westen 2000, van Westen et al. 2006; Petley 1999; Dietrich et al. 2001; Guzzetti 2005; Alexander 2008; Carrara and Pike 2008; Thaiyuenwong and Maireang 2010; Muntohar and Liao 2010; Mergili et al. 2012). The statistical methods are mainly applied in combination with GIS for regional-scale analyses, while deterministic—or physically based—methods are used for local-scale analyses, either with GIS (mainly the infinite slope stability model) or without GIS (usually applied on vertical sections with circular or elliptic sliding surfaces). For overview publications, see Carrara et al. (1999); Guzzetti et al. (1999); van Westen (2000, 2006, 2008).

Many different techniques and methods have also been developed in recent years for slope stability dynamic deterministic or deterministic analysis: the infinite slope, Lisa model, Distributed Shallow Landslide Model (dSLAM/IDSSM), SHallow Landsliding STABILITY (SHALSTAB), Stability INDEX MAPping (SINMAP), Transient response, Transient Rainfall Infiltration and Grid-based Regional Slope-stability analysis (TRIGRS), Probabilistic infinite slope analysis (PISA), PROBability of STABILITY PCRaster GIS package (PROBSTAB) as synthesized in Safaei et al. (2011) and Roslee et al. (2012).

The aim of this study is to use a simple slope stability model (the *infinite slope stability model*) to create *spatial quantitative landslide susceptibility maps* and to test the applicability of the model in natural conditions at different scales (e.g., Montgomery and Dietrich (1994); Wu and Sidle (1995); van Westen et al. (1997); van Westen and Terlien 1996; Gorsevski 2002; Crosta and Frattini 2003; Chang and Kim 2004; Capparelli et al. 2009).

This study while confined to susceptibility maps (due to the spatial distribution of landslides that exist or can occur in an area) does not take into consideration the temporal probability of a landslide event occurrence caused by the precipitation–slope instability modelling, using rainfall scenarios.

The model can be used in GIS software, because the calculation is done on a pixel basis. Each pixel acts as an entity and the effects of the neighboring pixels are not taken into account (e.g., van Westen and Terlien 1996).

Despite scientific literature cited in the previous paragraphs evidencing wide interests in the field, we consider that there are insufficient applied studies. It is necessary to have as many studies applied to as many geographic diverse environments as possible in order to test the applicability and limitations of the infinite slope stability model, as they will be stressed out in the “Result” and “Final remark” sections of this paper.

2 Study area

A landslide-prone area in Romania, located in the Subcarpathian sector of the Prahova River, was selected for this approach (Fig. 1). The Subcarpathians area is a hilly region of

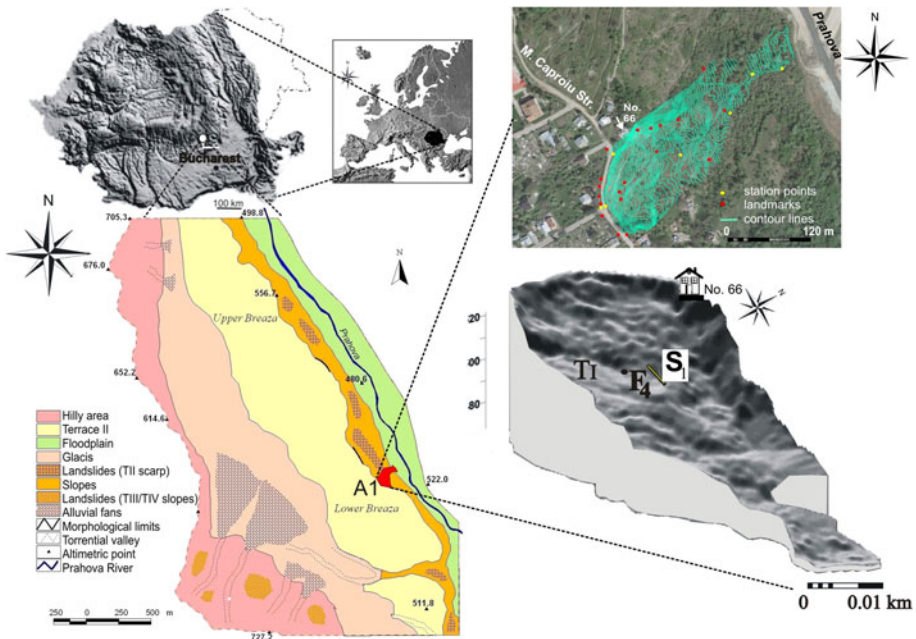


Fig. 1 Study area and active landslide *A1* location. Location of *F_d* drilling and *S₁* ditch in the *A1* landslide perimeter (*TII*, *TI*—terrace surfaces)

Romania situated outside the Carpathian arch, characterized by high tectonic instability and alternating permeable/impermeable rocks that favor active landslides. In this study, landslides were defined as gravitational downslope slid of an earth or rock mass (e.g., Varnes 1978; Cruden and Varnes 1996; the Unesco Working Party on the “World Landslide Inventory”—WP/WLI 1990, 1993; Highland and Bobrowsky 2008).

The field studies carried out during a period of 7 years along the Subcarpathian Prahova Valley allow for a wide-picture understanding of the active landslide processes, as well as the identification of the local lithological and structural settings.

The study area is the Breza syncline, a large syncline with a west-to-east orientation; it descends eastwards where has the widest extent. The syncline has symmetrically developed flanks and is axially faulted. The southern compartment of the structure is uplifted along a fault—the Breza fault (Fig. 2). The geological formation of Brebu conglomerates is present in the flanks of Breza syncline (Armaş et al. 2003).

Under these geological conditions, Prahova River, with a N–S oriented valley, has developed a large erosive basin. Prahova River carved four terraces, which are best preserved on the right valley side. Terrace II, named Breza terrace, is very wide reaching about 2 km at its maximum with absolute altitudes ranging from 500 to 550 m and situated approximately 60 m above the present riverbed of Prahova River. In the scarp of terrace II, the geomorphologic analysis led to the identification of a layer that represents terrace I, at a relative altitude of about 30 m (Fig. 1). The geotechnical survey carried out in the summer 2008 in the southern flank of the syncline confirmed the level of the terrace I under the active landslide material (Fig. 3).

The soil types are represented mainly by cambisols, followed by luvisolic soils, hydrosols, and protisols, with a depth between 0.5 and 2.5 m. The majority of soil types (42 %), on the surface, present a medium grounded texture (claysandy soils), followed by

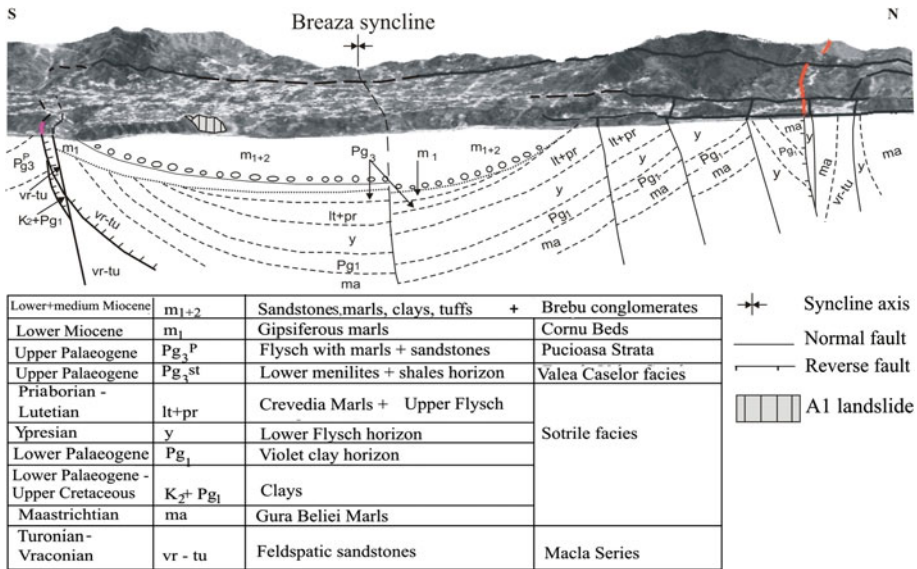


Fig. 2 Lithological profile of Breaza syncline (after Armaş et al. 2003)

medium-to-medium-fine grained texture (clay-claysandy) located in the colluvial–proluvial glacia. The soils’ permeability in the glacia area and on the Breaza terrace scarp is reduced (Parichi et al. 2006).

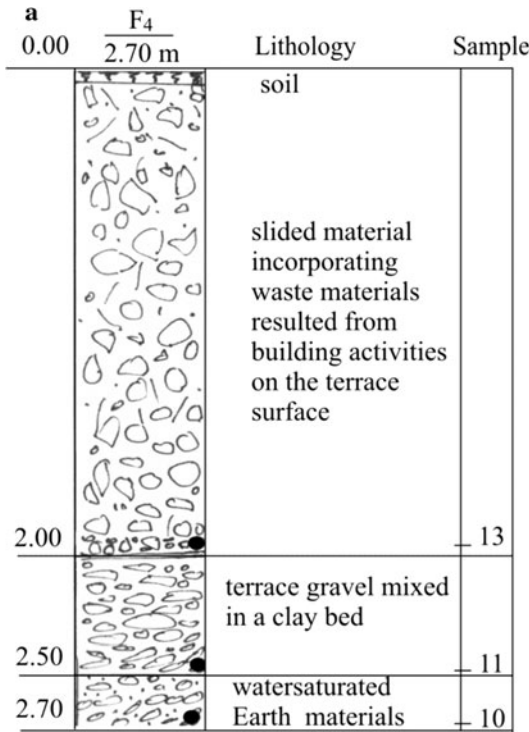
The measurements taken in 2008 in over 50 water wells identified the water table between 0 and 5 m underground. About 25 % of the study area is characterized by a very shallow water table, between 0 and 1 m, and half of it is located in the colluvial–proluvial glacia foot. The terrace’s tread is characterized by areas where the water table varies between 2 and 3 m in depth (29 %).

Shallow-to-medium deep landslides, both new and reactivated, dominate the scarps (affecting over 57 % of scarps surfaces) and are the characteristic for a 7–15° scarp gradient. Reactivations are found in the lateral crevices of the older landslides. Some of these landslides were naturally stabilized, especially by the planted gardens surrounding the built-up areas, natural grasslands, or orchards. However, where the land was used for intensive grazing, cattle steps prevented deepening of the natural drainage network, which could stabilize the versant through slipping water drainage.

The terrace II scarp has been shaped by a complex series of active landslides. In the second part of the study, we focused on the main A1 active landslide (see 2.1 and Fig. 1), which was used to test the model at a detailed scale in the second part of the analysis.

The slope is fragmented by amphitheater-shaped landslide heads, 5–8 m high. The displaced material forms forested slide waves, covered by willows (*Salix* species, the endemic species for the temperate continental climate rivers). Erosion reactivation, tension cracks, and slow movements appear especially in rainy years, affecting transport infrastructure. As a consequence, the width of the road is reduced, locally to less than 2 m. Under special rainy conditions, parts of the road are affected by mudslides or even mudflows.

Breaza town was developed on the tread of the terrace II and recorded an urban expansion by 0.5 % between 1984 and 2000, one of the highest values for the urban areas developed along the Subcarpathian Prahova River Valley. The constructions cover 45 % of the terrace tread and 13 % of the glacia from the upper terraces print foot.



b

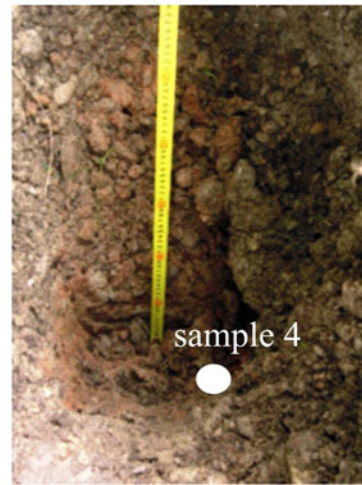
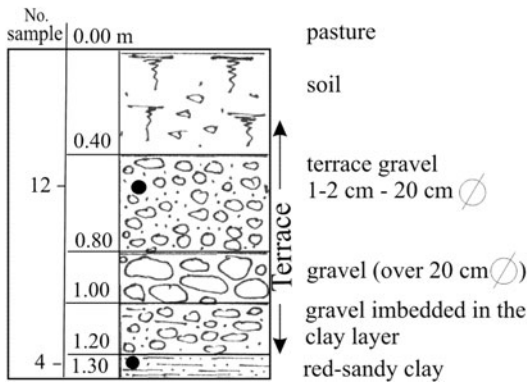


Fig. 3 Stratigraphic sections in the perimeter of A1 landslide. The landslide material has a thickness measured at 2.45 m at the F_4 drilling (a). At the S_1 ditch, dug on a geomorphologic surface in relation to the level of terrace I, there was identified and measured terrace material 2.30 m thick, placed directly on micaceous red sands 9 (b); 13, 11, 10, 12, 4 are rock samples

After 1990–1992, new constructions were built (Vartolomei and Armaş 2010) such as substantial weekend and holyday properties of one and two storeys with the ground floor partially dug into the substrata of the hill (Fig. 4).

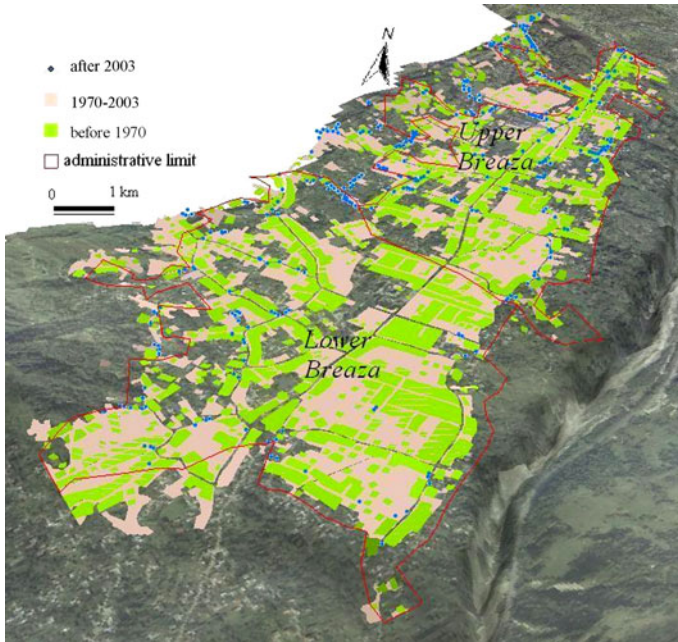


Fig. 4 Construction of houses evolution map

The extension of built-up area after 1990 without the necessary preliminary infrastructure development and problems such as increased traffic, the impact of the new buildings and infrastructure on the river's terrace edge, inappropriate sewage, and water drainage were completely ignored.

Many new constructions were built without proper structural foundations and frequently lacking feasibility studies. Furthermore, there are no feasibility studies concerning the load implied by the new constructions and the excavated materials from the scarp, nor studies concerning the drainage of pluvial water and subsequent constructions associated with domestic water collection (improper sewage pipes and septic tanks). The construction of these buildings on the edge and scarp of terrace II and all the trenches made for the foundation/walls and the underground cable and pipes represented the man-induced conditioning factors that favored the landslides of 1992, 1997, and autumn 2005 (Stroia et al. 2005). However, in the model presented in this paper, we did not consider the additional load induced by the construction of these new buildings.

An important triggering factor of landslides in the area of terrace II scarp is the running pluvial water on the streets perpendicular to the body of the scarp. These streets do not have a sewage system and are situated on a slope gradient of approximately 3° . All the water is discharged on the margin of the scarp or it infiltrates (with suffusion effects) in the last meters through the street infrastructure and through tension cracks parallel to the scarp. Consequently, these tension cracks are signs of a continuous dynamic opening and deepening process. At the base of the active landslide head, small pools appear in the rainy periods. The analysis made on a 15-year period (1990–2005) between the monthly quantity of precipitations, and the start of sliding processes, shows a slightly positive correlation of +0.3, significant at the 0.01 level (two-tailed).

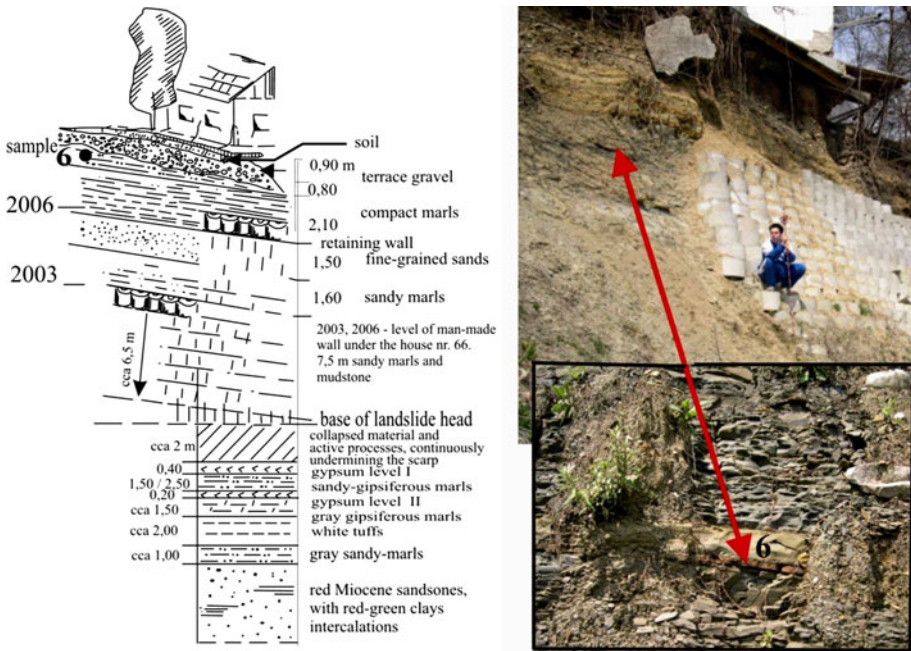


Fig. 5 Outcrop formed under the number 66 house (A1 landslide). The failure of the scarp in 1992 led to the present state, the construction being undermined on 1/5 of its surface and suspended on a width of 1.5 m above an almost vertical failure wall

2.1 Lithological local particularities and geotechnical characteristics of terrace II scarp

In the scarp of the Breaza terrace, there are geological sedimentary formations, which are stratified in centimetric and decimetric layers differing from the material used for the infrastructure and foundation of the old streets.

The terraces deposits buried by the active landslide mass (characterized by an active water circulation) are characterized by the presence of a type of limestone nodular material with a granular concentric structure on the surface of the terrace gravels (Armaş and Damian 2006).

This aspect was observed on the gravel samples taken from 2.40 m depth in the F_4 drilling, dug in the central sector of the active landslide.

By mapping the terrace scarps, in the section uncovered by failures, the geological characteristics of the layers from this flank of the Breaza syncline could be observed in detail (Fig. 5).

There are sedimentary formations, stratified in centimetric and decimetric strata, made of flint, clay, tuff, and gypsy–ferrous marls. At the base of the succession, there are solidified red sands bearing mica. In a dry state, they have a consistency index of a *solid rock*. Toward the edge of the landslide, the material dug from ditches showed slide masses of 1.5- to 2 m thick and the bed of the slide, formed by red sands with centimetric pellicles of clay.

The existence of the clay pellicles and the contact with the active water on these interfaces lead to the formation of a soft, slippery material. The presence and the type of the clay classify these rocks as “earths with swellings and strong contractions.”

The geotechnical indices are related to the presence of some hygrophilous minerals—illite and montmorillonite—which increase in volume in contact with water. The geotechnical characteristic mark reveals clay that stands at the “very active” limit.

In a wet state, the resistance parameters of this lithological strata decrease consistently. As a result, the rock layers above slid. That is why we took sample 4 from this decomposing layer and created a specific scenario on which the safety analysis was based (Fig. 3; Table 3).

3 Data

In this paper, we used the simple slope stability model to calculate safety factor maps for dry and saturated conditions, as well as for the groundwater high level scenario of 2008, according to the geotechnical data.

The infinite slope stability model is only suitable for shallow translational slope failures, under the assumption of an infinitely large failure plane, i.e., no variation of the “ox” axis (van Westen et al. 2006; Avanzi et al. 2009). The water table is assumed to be also parallel to the surface and the thickness of the soil mantle has to be much less than the length of the slope. In the research area, the geometric characteristics of the observed landslides are given in Table 1 and Fig. 6. The length-to-depth ratio in Table 1 shows that many landslides in the area can be considered as shallow, and consequently, the infinite slope stability model is a valid option.

Soil cohesion, unit weight, and internal friction angle for the geological formations from the study area are synthesized in Table 2.

The geotechnical properties of 50 rock samples from the sedimentary formation of Breaza syncline were analyzed indicating that materials are represented by clayey, silty-to-sandy clay, which are characterized by medium-to-high plasticity values.

The variables used for the infinite slope stability model are shown in table 3—sample 6 is clayey sand, according to granulometry analyses, and sample 4 is sandy silt. The reason why these two samples were selected to build the model is because they represent the slip surfaces in the area of terrace II scarp.

4 Method

In this paper, we used one of the simplest one-dimensional infinite slope stability modelling to compute the factor of safety (FS).

The factor of safety (FS) represents the ratio between stabilizing and destabilizing forces and was calculated by the infinite slope method given by Skempton and DeLory (1957), and resumed by Brunsdon and Prior (1984) (Eq. 1). Rock mass deformations are generated by effective stress (from grain to grain) and after elimination of pore water (Terzaghi 1925, 1943). Eq. 1 is written in effective stresses (c') without pore water pressure.

$$FS = \frac{c' + (\gamma + m\gamma_w)z \cos^2 \beta \tan \phi}{\gamma z \sin \beta \cos \beta} \quad (1)$$

where FS is the factor of safety, c' is the effective cohesion (N/m²), γ is the unit weight of soil (N/m³), m is the ratio between the groundwater level and the effective soil depth (z_w/z),

Table 1 Geometric characteristics of observed active landslides on terrace II slope

| No. | Length (m) | Width (m) | | | Depth (m) | | | Area (m ²) | Length-to-depth ratio | Volume (m ³) |
|-----|------------|-----------|--------|--------|-----------|--------|--------|------------------------|-----------------------|--------------------------|
| | | Average | Maxima | Minima | Average | Maxima | Minima | | | |
| A1 | 353 | 124 | 185 | 63 | 4.25 | 8 | 0.5 | 34,286 | 44.12 | 41,175 |
| A2 | 333 | 192 | 228 | 156 | 4.85 | 9 | 0.7 | 63,436 | 37 | 123,300 |
| A3 | 386 | 128 | 177 | 80 | 2.65 | 5 | 0.3 | 50,343 | 77.2 | 36,325 |
| A4 | 368 | 162 | 235 | 89 | 4.25 | 8 | 0.5 | 69,253 | 46 | 59,825 |
| A5 | 267 | 129 | 190 | 69 | 7 | 13 | 0.9 | 40,758 | 20.53 | 253,750 |
| A6 | 229 | 96 | 128 | 64 | 6.4 | 12 | 0.8 | 25,973 | 19.08 | 142,300 |
| A7 | 270 | 316 | 362 | 270 | 8 | 15 | 1 | 74,244 | 18 | 429,225 |
| A8 | 337 | 141 | 200 | 83 | 8.5 | 16 | 1 | 44,990 | 21.06 | 235,300 |
| A9 | 161 | 69 | 84 | 54 | 6.9 | 13 | 0.8 | 11,853 | 12.38 | 66,900 |
| A10 | 164 | 63.5 | 91 | 36 | 7.35 | 14 | 0.7 | 11,546 | 11.71 | 57,625 |
| A11 | 177 | 95.5 | 136 | 55 | 6.3 | 12 | 0.6 | 18,700 | 14.75 | 89,125 |
| A12 | 116 | 47.5 | 66 | 29 | 5.2 | 10 | 0.4 | 7,070 | 11.6 | 31,600 |
| A13 | 176 | 82 | 100 | 64 | 7.35 | 14 | 0.7 | 14,613 | 12.57 | 51,875 |
| A14 | 200 | 50.5 | 71 | 30 | 4.75 | 9 | 0.5 | 11,868 | 22.22 | 30,950 |
| A15 | 102 | 61.5 | 73 | 50 | 4.7 | 9 | 0.4 | 6,082 | 11.33 | 23,075 |
| A16 | 92 | 61 | 92 | 30 | 5.5 | 10 | 1 | 8,003 | 9.2 | 58,550 |
| A17 | 181 | 80 | 106 | 54 | 1.6 | 3 | 0.2 | 15,073 | 60.33 | 3,825 |

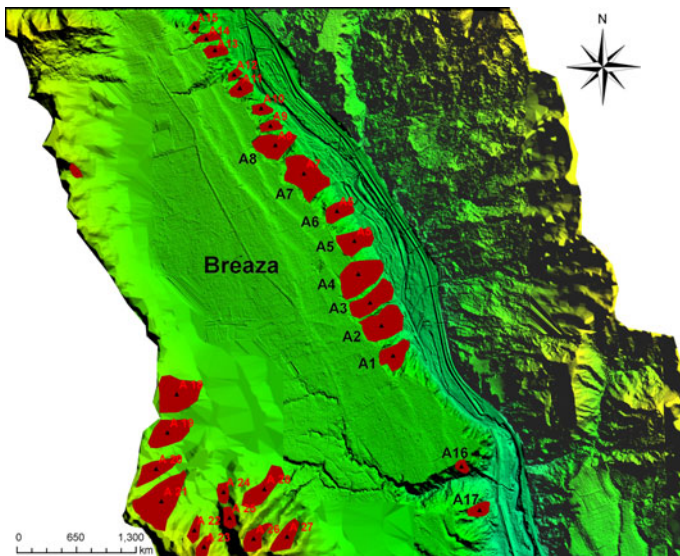


Fig. 6 Location of landslides in the study area superposed on LIDAR-DEM (2012)

γ_w is the unit weight of water (N/m³), z is the thickness of soil above the failure plane (m), z_w is the height of water table above failure surface (m), β is the slope angle (°), and φ is the angle of internal friction (°).

Table 2 Characteristics of the geological formations from the study area

| Lithology | Cohesion (kN/m ²) | A unit weight of soil (kN/m ³) | Internal friction angle Φ (°) |
|---|-------------------------------|--|------------------------------------|
| Brebu conglomerates | 8,000 | 24 | 56 |
| Fusaru sandstones (Pucioasa Strata) | 6,000 | 23 | 40 |
| Miocene sandstones | 7,000 | 23 | 45 |
| Calcareous marls (Sotriale facies) | 2,600 | 27 | 34 |
| Cornu beds (marls, clays) | 3,300 | 20 | 51 |
| Clays and marls from the miocene sedimentary filling of Breaza syncline | 2,400 | 20 | 20 |

Medium relative values obtained from the scientific literature (Teodorescu 1984) or collected from mines (mining and drilling) and own field studies

Table 3 Values and range of parameters used in the model

| Sample 6 | Values |
|--|--------------------------------|
| Slope β (°) | Area with values range 0–81 |
| Cohesion c (Pa = N/m ²) | 50,000 |
| Internal friction angle Φ (°) | 30 |
| Tan Φ | 0.577 |
| Unit weight of water γ_w (N/m ³) | 10,000 |
| Unit weight of wet soil γ_t (N/m ³) | 19,000 |
| Submerged unit weight γ' (N/m ³) | 17,000 |
| Unit weight of saturated soil γ_{sat} (N/m ³) | 20,000 |
| Soil depth z (m) | Area with values range 0.4–2.5 |
| Saturation ratio m | 0–1 |
| Sample 4 | Values |
| Slope β (°) | Area with values range 0–86 |
| Cohesion c (Pa = N/m ²) | 20,000 |
| Internal friction angle Φ (°) | 23 |
| Tan Φ | 0.424 |
| Unit weight of water γ_w (N/m ³) | 10,000 |
| Unit weight of wet soil γ_t (N/m ³) | 19,000 |
| Submerged unit weight γ' (N/m ³) | 18,000 |
| Unit weight of saturated soil γ_{sat} (N/m ³) | 20,500 |
| Soil depth z (m) | Area with values range 1–3 |
| Saturation ratio m | 0–1 |

A description of the data used in this study is given in Table 4

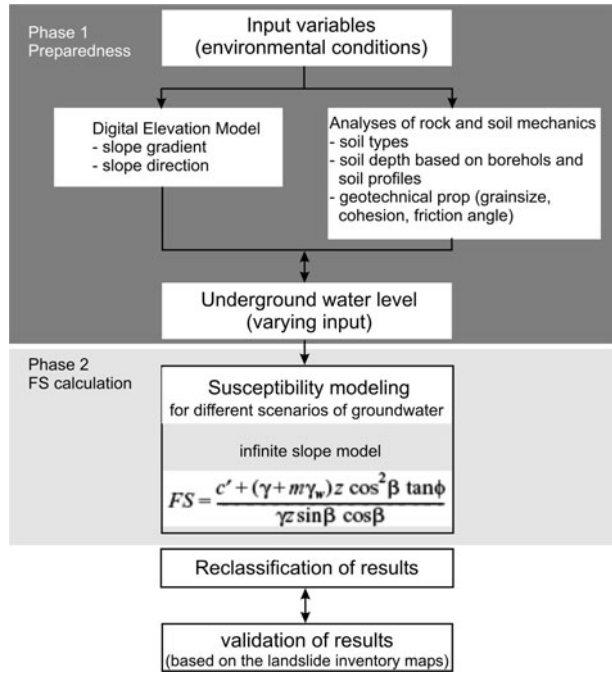
Slope stability is a direct function of soil's shear resistance, given by c and Φ . In order to distinguish the contribution of soil cohesion and of the internal friction angle to the safety index, we applied the two indices used by Chang and Kim (2004, p. 420):

$$FS = I_1 + I_2 \quad (2)$$

Table 4 Input data and parameters

| Data | Data format | Use | Sources |
|--|----------------------------|--|---|
| Imagery | Raster | Orthophotoplan images (2012), topographic maps 1:25,000 and 1:5,000 (1980), historical maps, LiDAR (2012). Derivation of elevation models, slope parameters, landslides map, etc | Military Topographic Directorate, National Geodesic Fund, etc |
| Digital elevation models | Raster | To calculate landslide volumes and topographic changes by subtracting terrain digital models from different years | The 1980 DEM resulted from the digitized contour (1: 25,000 topographic map). The 2001–2003 DEM resulted from the topographic surveys carried out in the same period and the 2012 DEM extracted from the 2012 LiDAR |
| Topographic surveys | Vector (point) | To obtain the DEM, the groundwater depth map and the thickness of soil layers map | Field surveys carried out with the total station and the GNSS technologies |
| Geological and geomorphologic maps | Spatial and tabular | Identification of the local, geomorphologic, lithological, and structural setting | Field surveys |
| Geometric characteristics of landslides | Tabular | Analysis to test the applicability of slope stability model | Field surveys, map analysis, and subtraction of DEMs |
| Geotechnical data (indices and parameters) | Tabular | Data input for the infinite slope model | Mapping, sampling, and laboratory analysis; literature values |
| Soil parameters (texture, permeability, etc.) | Tabular and vector (point) | Data input for the infinite slope model | Field sampling and laboratory samples analysis |
| Water table measured in over 50 water wells (2008) | Tabular and vector (point) | Data input for the infinite slope model | Field surveys |

Fig. 7 Flow chart scheme of the deterministic approach



where

$$I = \frac{c}{[(1 - m)\gamma_t + m\gamma_{sat}]z \sin \beta \cos \beta}$$

$$I = \frac{[(1 - m)\gamma_t + m\gamma']}{[(1 - m)\gamma_t + m\gamma_{sat}]} \cdot \frac{\tan \phi}{\tan \beta}$$

c : cohesion (t/m^2) γ_t : unit weight of moist soil (t/m^3) γ' : submerged unit weight (t/m^3) γ_{sat} : saturated unit weight of soil (t/m^3) Slope stability depends upon the saturation degree, so that an important factor of the FS equation is the ratio between the underground water level and the soil depth, m . This ratio is 0 when the soil is completely dry, and this is the most favorable condition. The ratio is 1 when the soil is completely saturated. The saturation depth “ m ” is weather-dependent, and the fact that rainfalls are the most important triggering factors for shallow active landslides is very well researched and documented in the well-renown literature in the field (e.g., Yong et al. 2005; Bozzano et al. 2007; Travalletti et al. 2008). In this study, we tested two simulated situations, $m = 0$ and $m = 1$, and one real condition based on the groundwater table mapped in summer 2008. The water table measured in summer 2008 is not relevant for the occurrence of landslides, but it rather reflects the average conditions with an index of precipitation sum of 709.2 mm/year (annual total precipitation amount in the area is 779 mm/year for the period 1961–1990).

The model was generated as an ILWIS (Integrated Land and Water Information System) function, where the different scenarios were calculated by changing the variables of the function. Because the method was integrated with a raster-based GIS (ILWIS), every term in Eq. 1 became a space variable. The underground water level ratio, the “saturation” depth “ m ,” is the only time-dependent variable. For each pixel, calculations resulted in a safety factor value.

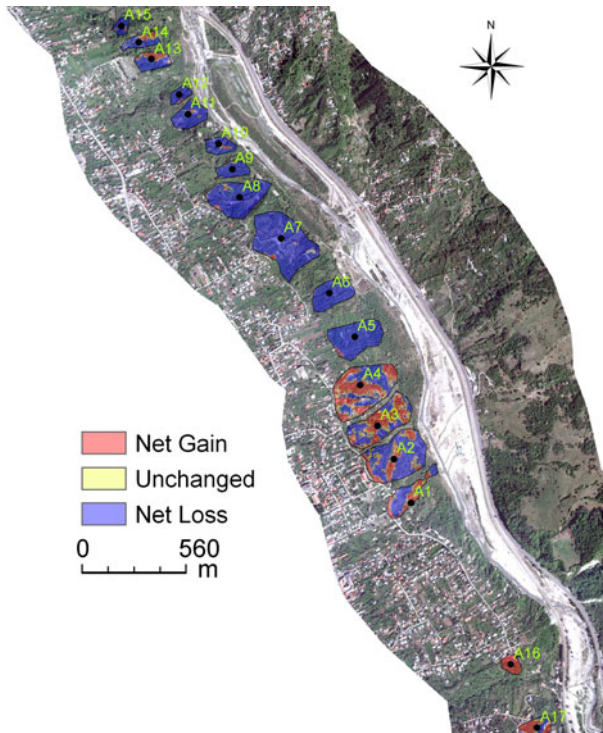


Fig. 8 Variations of topography resulted from DEMs subtraction for terrace II slope (1980–2012)

The methodological flow chart for this study is shown in Fig. 7 and is differentiated in two phases: the preparation phase and the analytical phase.

The preparation phase included geological and geomorphologic field work, interpreting of aerial photographs and historical maps, shallow excavations, trenches, and boreholes; over 50 samples for geotechnical analyses were collected (Armaş et al. 2003; Armaş and Damian 2006; Parichi et al. 2006). Variations of topography for the period between 1980 and 2012 and landslide volumes were quantified based on DEMs subtraction, using Cut/Fill operation in ArcScene GIS—the DEM maps obtained from the large-scale topographic maps (1980), the topographic field measurement implemented during 2001–2003, and the latest DEM obtained through LIDAR raster at a resolution of 1 m (2012). The terrain digital models used were brought to the same resolution and the same number of rows/columns.

Fig. 8 is an example of the situation for the terrace II slope. The accumulations from the detaching landslide heads are due to man-induced causes, which for the time period considered (1980–2012) consisted of slopes strengthening by filling the ravines with soil, gabions, concrete walls to protect the road (Miron Caproiu Str.), all these works leading to an upload of the land.

For this research, we mapped soil types and measured soil thickness through 36-point measurements and soil profiles uniformly distributed in the research area (Fig. 9). The underground water table was mapped in 50 water wells in the summer of 2008. The data collected during the field trip campaigns using GPS were imported in ArcGIS and converted using the Point to Polyline function (Edit Tools extension). Existent vector data

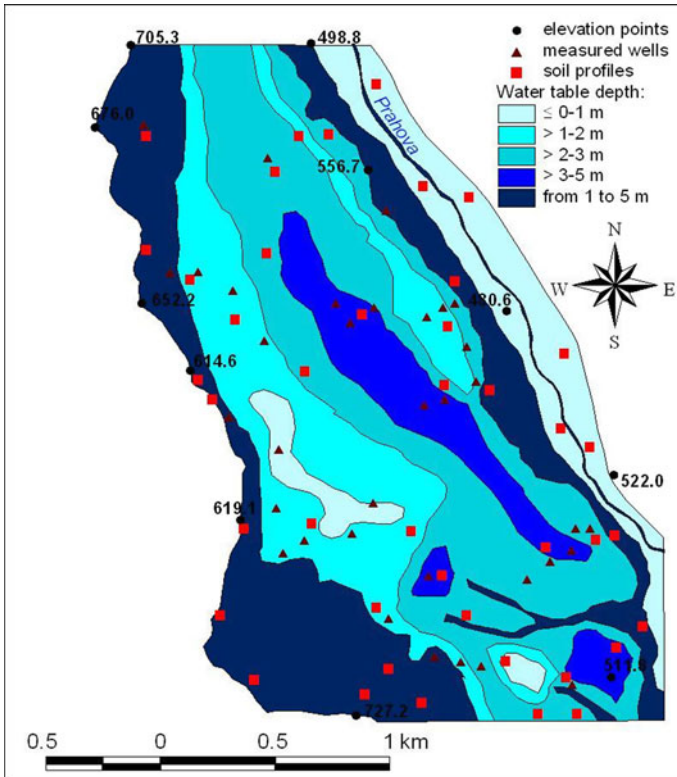


Fig. 9 Water table map with soil profile and water wells positions

were transferred into raster using GRASS software through *File—Map type conversion—Vector to raster* (function—*v.to.rast*). By using *r.surf.contour*, all maps were created one by one with the linear interpolation method including a phreatic depth map and a soil layer thickness map. The exported maps, through *File—Export raster map—ESRI ASCII grid export [r.out.arc]*, were processed by ArcScene GIS (and for comparison in Global Mapper).

Several maps were geo-referenced, so that they could be tied to the same projection system, and were implemented into ILWIS-GIS software.

The Digital Elevation Model (DEM) of the study area was obtained by interpolation of the contours from topographic maps 1/25,000 and 1/5,000, at 10- and 5-m intervals, corroborated with the high-resolution digital elevation map generated by airborne LIDAR (2012) for the scarp of terrace II. Different terrain attributes, such as slope gradient and the sine and cosine of the slope, were derived from further processing of the DEM in the ILWIS software. Landslide susceptibility was determined using slope stability model, based on slope parameters (cohesion, angle of internal friction, specific weight), soil thickness, and ground water level measured during the summer of 2008 field campaign (Fig. 9). Unfortunately, for the area of study, we could not use available recent geotechnical data; therefore, our model was based on a few field-sampled data and theoretical scientific papers (Teodorescu 1984). This aspect can hypothetically become a major drawback of the model, as pointed later in the paper.

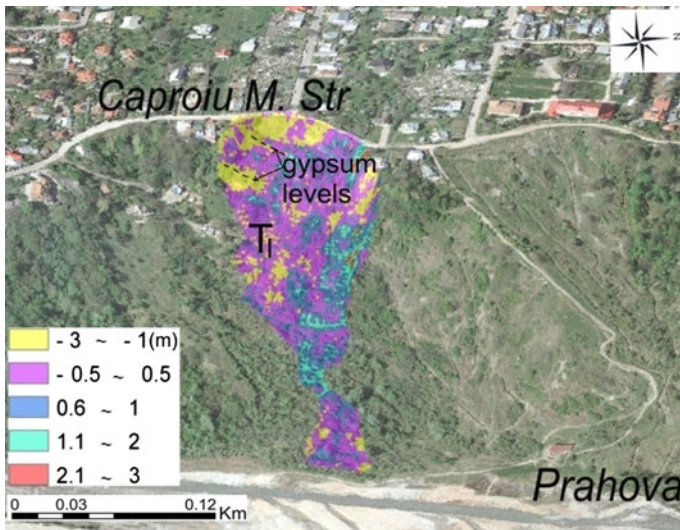


Fig. 10 3D result of DEMs subtraction for A1 landslide

The last step of the analysis was to classify the calculated maps into three stability classes. When the calculated FS is over 1.5, the slope is in a stable condition, only major destabilizing factors leading to instability. When FS is less than 1, the slope is in an unstable condition. If the FS is equal to 1 or less than 1.5, the slope is at the point of failure or in a quasi-stable condition, and minor destabilizing factors can lead to instability.

To check the conditions of scale detail for which the method operates better, we applied the slope stability model (the methodological steps indicated in Fig. 7) in different scenarios of hydrological conditions on the A1 landslide. The landslide is over 360 m long and 120 m wide, with a general 15° slope gradient (Fig. 1; Table 1). The first topographic field works were carried out in 2002 and 2003 using a total station Leica TC 805 (Leica Geosystems ©) and drawing 1/5,000 scale maps (Armaş et al. 2003). Four station points were taken on the A1 landslide body, recording 6,000 elevation points on a 34,286 m² slid surface. In the autumn of 2012, the active landslide was topographically mapped with Topcon GR-3 state-of-the-art equipment, using the RTK-Cinematic method in real time and differential real-time corrections provided by the specialized ROMPOS (Romanian Position Determination System) service. Data downloading and processing were performed with geodetics software and imported into ILWIS-GIS. The distribution of the thickness of material in A1 landslide was measured in several key points through drillings and ditches in the field campaigns of 2007 and 2008. Figure 10 represents the topography variations of A1 landslide based on DEMs subtraction for the period between 2002 and 2012.

5 Results

The safety factor based on the relationship between soil thickness, groundwater, and slope angle is highlighted in the susceptibility maps illustrated in Fig. 11 (calculations were carried out based on sample 6 parameters). As seen from the cartographic results, most of the areas with low safety factors are situated on steeper slopes.

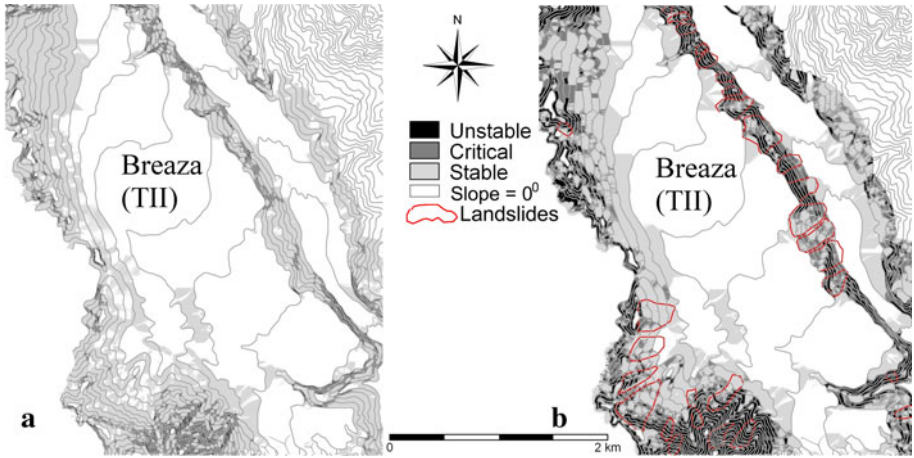


Fig. 11 Unstable areas predicted by the slope instability model under dry (a) and saturated (b) conditions. As a general rule, FS is decreasing when slope gradient gets higher and when assuming fully saturated soil. Active landslides sites (b)

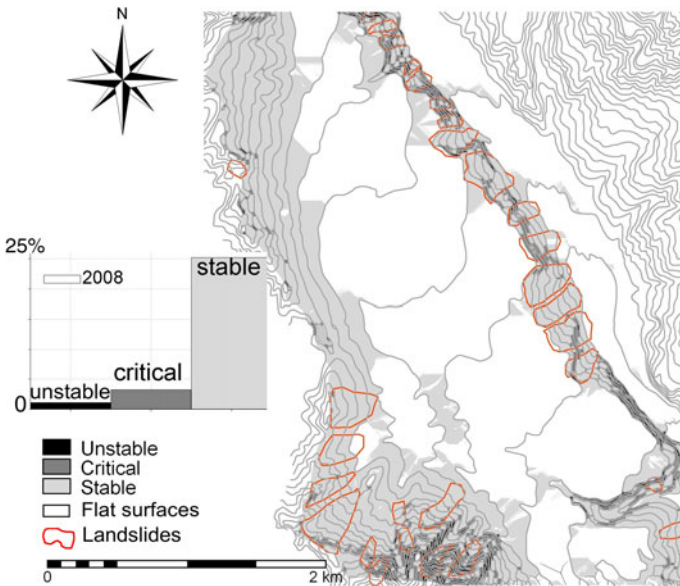


Fig. 12 Unstable areas predicted by the slope stability model under the conditions of summer 2008. The histogram indicates the percentage area under different stability classes

The results for the computation with the measured water table of summer 2008 are shown in Fig. 12. For both computations shown in Figs. 11 and 12, we assumed that the sliding surface coincides with the bottom of the soil.

The unstable areas predicted by the slope stability model are similar to the observations in the field, with a higher susceptibility to landslides predicted on the southern wing of the syncline, where landslide scarps are deeper, on layers front.

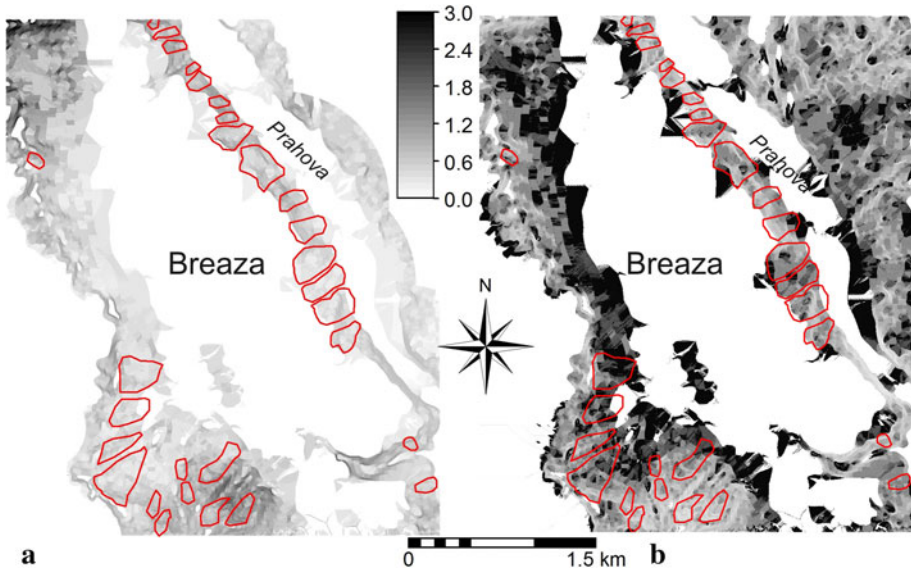


Fig. 13 Index₁ (a) and Index₂ (b) for saturated soil conditions ($m = 1$)

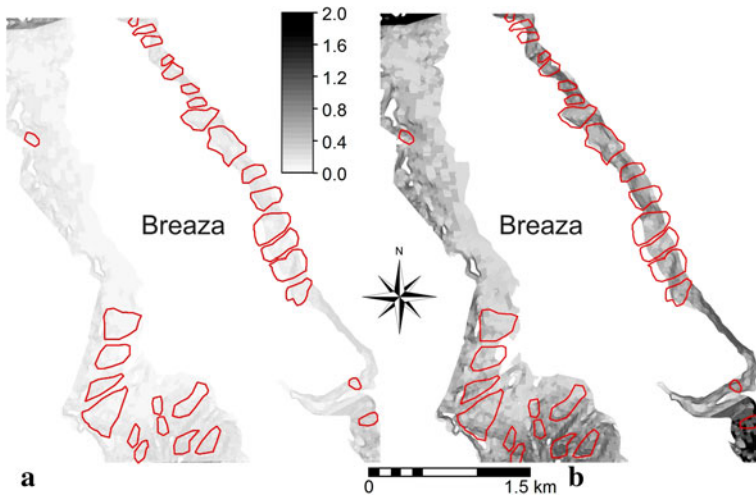


Fig. 14 The importance of soil depth for FS in saturated soil conditions **a** shallow soil depth, 0.5 and **b** 2 m soil depth

The strata fall with a higher angle toward the topographic slope to the syncline axis (Fig. 2). In the northern flank of the syncline (Brebu conglomerates outcrop), the landslides are shallower and mostly stabilized, by the prevailing drainage process.

The transition from the upper terrace slope to the accumulating glacis that occupies the terrace II tread is also clearly sketched in Fig. 11. Terrace II slope is fragmented in a succession of gliding basins tied with steps and movements corresponding to different landslide generations. The remnant shoulder level of terrace I can be seen as a stability

pattern on the slope of terrace II. Pearson's correlation (SPSS program) is significant for statistics between the mapped landslides and the stability factor at a critical level, or instability in a scenario when slopes are completely saturated: $r = 0.845$; sig. (two-tailed) = 0.01.

In Fig. 13 are reproduced the two indices used by Chang and Kim in (2004), for a saturated soil. Index 1 emphasizes the cohesion of soil in the equation of safety factor, and index 2 shows the internal friction.

According to Chang and Kim (2004), the soil cohesion becomes a more important factor for slope safety in conditions of shallow soil depth and increasing slope gradient. By applying different soil cohesion conditions averagely specific in the study area (Table 2), it can be observed in Fig. 14a and b the FS variation in saturated plain for shallow and deep soils. The values of the indices are decreasing significantly in the scenario of soils with depths of 0.5 m (Fig. 14a) compared with the scenario in Fig. 14b, where the soils were supposed to have a 2 m depth.

Index I_2 is affected by changes in slope gradient and the internal friction angle. Slope stability increases when the slope angle β decreases. As a general rule documented by Chang and Kim (2004) and observed also in our research, the underground water ratio becomes critical to slope stability in the slopes areas with deep soils. Under these conditions, rainfall quantities gain importance. As already Crosta and Frattini mentioned in (2008), soil cohesion is more variable than the friction angle. Moreover, the factor of safety is more sensitive to the cohesion spatial variations than to the friction angle, and wetting conditions emphasizes cohesion variability (Sidle 1984).

The next stage of the study was to focus the analysis at a scale of a representative landslide. For this, the southern flank of the syncline was chosen, where on the terrace II slope takes shape a specific morphologic and morphodynamic model of landslides, named as A1 in Fig. 1.

Four simulated situations of saturation ratio were tested: $m = 0$, $m = 0.3$, $m = 0.6$ and $m = 1$. Figure 15 shows only the results from dry and saturated conditions ($m = 0$ and $m = 1$), for the parameters derived from two different samples (samples 4 and 6).

Analysis results show valid consistency with the real landslide occurrence. In wet conditions, the instability is higher for the scenario based on sample 4. Sample 4 represents red sands with centimetric pellicles of clay that forms the bed of A1 landslide. For dry

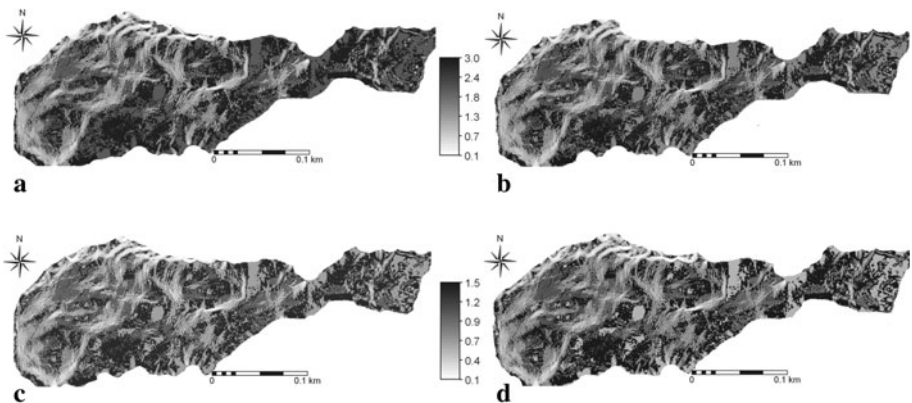


Fig. 15 Factor of safety under dry and saturated conditions, computed with parameters from sample 4 (a, dry; c, saturated) and 6 (b, dry; d, saturated)

conditions, the general patterns of both maps are the same. The result is being validated through geomorphologic field analysis.

The morphodynamic analysis shows a continuous retreat of the tension cracks during the 10 years (Fig. 10). The filling material of the Caproiu M. street breaks down in a ladder-like pattern, especially during the rainy seasons, when the surface drainage along the street is associated with a subterranean drainage (suffusion). The drainage is following the axis of the street. The gravitational process starts as falls, developing into translational slides. In the upper half of the landslide, the material moves along a direction controlled by two gypsum levels, then it is reoriented to the Prahova River. In the ledge, a secondary landslide head scarp developed.

There is also a relative stability period of the sliding process at terrace I level, at 30 m relative altitude (Fig. 10). Field observations during the study period showed a removal of the material from the slide waves through drainage on the structural surface, a pattern observed by the modelling of the safety factor, but also by the analysis of topographic variations.

At the base of the gypsum levels, there are medium-fine granular quartzous gritstones with carbonatic and gypsum cement, in centimetric layers, crossed apparently chaotic by fissures filled with gypsum and anhydrite. The dissolving process of this succession is favored by the infiltration of pluvial waters, but also by water redirected by construction works: foundations, water wells, septic tanks, and ditches for roads. Weathering causes gypsum minerals to dissolve determining the sliding process; this phenomenon was observed after the rainy period in September 2005.

This concordance of modelled results with field observations and the computation of topographic variations demonstrate that the model functions better for a large-scale analysis.

Validation of results for the entire area was made under the assumption that landslides are related to spatial information, using known landslide locations. For the validation process, only the scarps of superficial translational landslides were selected from the landslide distribution maps. The resulting map was crossed with the safety factor maps to create the success rate (Chung and Fabbri 2003). Best performance is achieved when the success rate captures the majority of the mapped landslides scarps in the pixel area classified as unsafe and is furthest removed from the 1:1 line that represents a random model (Ulmer et al. 2009). We assumed fully saturated conditions (from rainfall or anthropogenic reasons) as relevant for landslide initiation and evaluate the model with the results shown in Fig. 11b. The quite-low classification power of the model used has two causes. First, this is because the model was developed on the hypothesis of a unique sliding bed, and this assumption representing an unacceptably high degree of generalization for a model so sensitive to the input conditions. The low classification power of the model results also in the high number of false positives (error type I—Tables 5, 6) grouped on the abrupt versants of the defile carved into the Brebu conglomerate. The gorge carved in the southern flank of Breaza syncline has specific geological and geomorphologic characteristics differing from the rest of the study area, and the model would have a much better classification power if the gorge sector was excluded. Conglomerate and sandstones crop up on the Breaza syncline flanks and Prahova River carves in these strata, a relief of abrupt versants. On the southern flank of the syncline, the abrupt versants are affected by torrents, the reception pools of the torrents being feed through suffusion, and creek processes developing on the edge of terrace II slope.

However, the false negatives (non-observations of the dangerous phenomenon = 0.24 %) show that the model has been able to correctly classify safety areas.

Table 5 Prediction errors (% of correctly and incorrectly predicted pixels)

| Predicted | Observed | |
|----------------------|-------------------|---------------------------|
| | Correctly | False positives/negatives |
| Positives (instable) | 1.9 (<i>a</i>) | 44.76 (<i>b</i>) |
| Negatives (stable) | 53.1 (<i>d</i>) | 0.24 (<i>c</i>) |

Table 6 Accuracy statistics derived from Table 5

| | | |
|--|---|------|
| Efficiency $a + d$ | % of correctly classified pixels | 55 |
| Misclassification rate $b + c$ | % of incorrectly classified pixels | 45 |
| Odds ratio $(a + d)/(b + c)$ | Ratio between correctly and incorrectly classified pixels | 1.22 |
| Positive predictive power $a/(a + b)$ | The proportion of true positives in the total of positive predictions | 0.04 |
| Negative predictive power $d/(c + d)$ | The proportion of true negatives in the total of negative predictions | 0.99 |

Another limitation of the model approach used, assumed in research, was the impossibility to include the influence of additional load induced by the construction of new buildings. This is because the aim of our research was to test the model only according to geotechnical parameters and soil depth conditions, without taking into consideration the load induced by constructions.

6 Final remarks

In this paper, we tested the applicability in GIS of the deterministic slope stability model for spatial landslide susceptibility in a hilly region of Romania.

The results have shown scale dependence of the applied safety model. Even if the slope stability model can provide scenarios of potential instability, it is difficult to apply it on large areas because it is very data-demanding, requiring a high degree of simplification of the input data, including landslides type and depth. Accuracy of input data is scale-dependent and influences the results. The wide variability in uncertainties in input parameters from site to site makes the relationship between FS and effective failure not trustable. In this case, using a single value for cohesion and internal friction angle leads to a great simplification of results, because the active landslides are happening and on the other strata then those used in the model. Our research results were confirmed on large-scale basis by field observation, underlining the usefulness of slope stability models for detailed analyses of potential instabilities.

A possible continuation of our work will be to monitor the development of the groundwater level in relation to rainfall and make the prediction directly with the slope stability model, based on changing groundwater level. By taking into account the different scenarios of severe rainfall conditions and adding temporal probability of landslide hazard events, susceptibility maps will be transformed into hazard maps.

Acknowledgments This research was partially supported by the National Research Council (CNCS) of Romania through the project No. 2916/31 GR, having prof. I. Armas as Principal Investigator. The authors wish to express their thanks to Dr. Martin Mergili from The Institute of Applied Geology in Vienna and to an anonymous reviewer for their valuable support and constructive comments on this paper.

References

- Alexander DE (1991) Applied geomorphology and the impact of natural hazards on the built environment. *Nat Hazards* 4(1):57–80. doi:[10.1007/BF00126559](https://doi.org/10.1007/BF00126559)
- Alexander DE (1992) The causes of landslides: human activities, perception, and natural processes. *Environ Geol Water Sci* 20(3):165–179. doi:[10.1007/BF01706160](https://doi.org/10.1007/BF01706160)
- Alexander DE (2008) A brief survey of GIS in mass-movement studies, with reflections on theory and methods. *Geomorphology* 94:261–267. doi:[10.1016/j.geomorph.2006.09.022](https://doi.org/10.1016/j.geomorph.2006.09.022)
- Armaş I, Damian R (2006) Evolutionary interpretation of the Landslides from the Miron Căprioiu Street Scarp (Eternităţii Street—V. Alecsandri Street)—Breaza Town. *Revista de Geomorfologie* 8:65–72
- Armaş I, Damian R, Şandric I, Osaci-Costache G (2003) Vulnerabilitatea versanţilor subcarpatici la alunecări de teren (Valea Prahovei), ed. Fundaţiei România de Măine, Bucharest
- Avanzi GA, Falaschi EF, Giannecchini ER, Puccinelli EA (2009) Soil slip susceptibility assessment using mechanical–hydrological approach and GIS techniques: an application in the Apuan Alps (Italy). *Nat Hazards* 50:591–603. doi:[10.1007/s11069-009-9357-4](https://doi.org/10.1007/s11069-009-9357-4)
- Brunsdon D, Prior DB (1984) Slope stability. Wiley, New York, 620pp
- Bozzano F, Cipriani I, Mazzanti P, Prestininzi A (2007) Displacement patterns of a landslide affected by human activities: insights from ground-based InSAR monitoring. *Nat Hazards*. doi:[10.1007/s11069-011-9840-6](https://doi.org/10.1007/s11069-011-9840-6)
- Capparelli G, Biondi D, De Luca D, Versace P (2009) Hydrological and complete models for forecasting landslides triggered by rainfalls. In: Proceedings of the first Italian workshop on landslides. Versace Università della Calabria, Rende, Napoli, pp 162–173
- Carrara A, Pike R (2008) GIS technology and models for assessing landslide hazard and risk. *Geomorphology* 94:257–260. doi:[10.1016/j.geomorph.2006.07.042](https://doi.org/10.1016/j.geomorph.2006.07.042)
- Carrara A, Guzzetti F, Cardinali M, Reichenbach P (1999) Use of GIS technology in the prediction and monitoring of landslide hazard. *Nat Hazards* 20(2–3):117–135. doi:[10.1023/A:1008097111310](https://doi.org/10.1023/A:1008097111310)
- Chang H, Kim NK (2004) The evaluation and the sensitivity analysis of GIS-based landslide susceptibility models. *Geosci J* 8(4):415–423. doi:[10.1007/BF02910477](https://doi.org/10.1007/BF02910477)
- Chung CJF, Fabbri AG (2003) Validation of spatial prediction models for landslide hazard mapping. *Nat Hazards* 30:451–472. doi:[10.1023/B:NHAZ.0000007172.62651.2b](https://doi.org/10.1023/B:NHAZ.0000007172.62651.2b)
- Crosta GB, Frattini P (2003) Distributed modelling of shallow landslides triggered by intense rainfall. *Nat Hazards Earth Syst Sci* 81–93. doi:[10.5194/nhess-3-81-2003](https://doi.org/10.5194/nhess-3-81-2003)
- Crosta PB, Frattini P (2008) Preface rainfall-induced landslides and debris flows. *Hydrol Process* 22(4):473–477. doi:[10.1002/hyp.6885](https://doi.org/10.1002/hyp.6885)
- Cruden DM, Varnes DJ (1996) Landslide types and processes. In: Special report 247: landslides: investigation and mitigation. Transportation Research Board, Washington DC
- Dietrich WE, Bellugi D, Real de Asua R (2001) Validation of the shallow landslide model, SHALSTAB, for forest management. In: Wigmosta MS, Burges SJ (eds) Land use and watersheds: human influence on hydrology and geomorphology in urban and forest areas, American Geophysical Union, Water Science and Applications 2:195–227. doi:[10.1029/WS002p0195](https://doi.org/10.1029/WS002p0195)
- EM-DAT (Emergency events database) (2006) OFDA/CRED Retrieved from International Disaster Database from <http://www.cred.be/emdat>, Université Catholique de Louvain, Brussels. Accessed March 2006
- Gorsevski PV (2002) Landslide hazard modeling using GIS. Ph.D. thesis, University of Idaho
- Guzzetti F (2005) Landslide hazard and risk assessment. Dissertation, Rheinische Friedrich-Wilhelms-Universität Bonn
- Guzzetti F, Carrara A, Cardinali M, Reichenbach P (1999) Landslide hazard evaluation: a review of current techniques and their application in a multiscale study, Central Italy. *Geomorphology* 31(1–4):181–216. doi:[10.1016/S0169-555X\(99\)00078-1](https://doi.org/10.1016/S0169-555X(99)00078-1)
- Highland LM, Bobrowsky P (2008) The landslide handbook—a guide to understanding landslides, 1325. US Geological Survey Circular, Reston, p 129
- Hoek E, Bray JW (1997) Rock slope engineering, 3rd edn. IMM E&FN Spon, London

- Mergili M, Fellin W, Moreiras St M, Stotter J (2012) Simulation of debris flow in the Central Andes based on Open Source GIS: possibilities, limitations, and parameter sensitivity. *Nat Hazards* 61:1051–1081. doi:[10.1007/s11069-011-9965-7](https://doi.org/10.1007/s11069-011-9965-7)
- Montgomery DR, Dietrich WE (1994) A physically-based model for the topographic control on shallow landsliding. *Water Resour Res* 30:1153–1171. doi:[10.1029/93WR02979](https://doi.org/10.1029/93WR02979)
- Munthohar AS, Liao HJ (2010) Rainfall infiltration: infinite slope model for landslides triggering by rain-storm. *Nat Hazards* 54:967–984. doi:[10.1007/s11069-010-9518-5](https://doi.org/10.1007/s11069-010-9518-5)
- Parichi M, Armaş I, Vartolomei F (2006) Pedological and morphodynamic aspects in Subcarpathian sector of Prahova Valley. *Analele Spiru Haret* 9:103–111
- Petley DN (1999) Failure envelopes of mudrocks at high effective stresses. In: Aplin AC, Fleet AJ, Macquaker JHS (eds) Physical properties of mud and mudstones. *Geol Soc Lond Spec Publ* 158
- Roslee R, Jamaluddin TA, Talip MA (2012) Intergration of GIS Using GEOSTATistical INTERpolation Techniques (Kriging) (GEOSTAINT-K). In: Deterministic models for landslide susceptibility analysis (LSA) at Kota Kinabalu, Sabah, Malaysia, *J Geogr Geol* 4(1):18–32. doi: [10.5539/jgg.v4n1p18](https://doi.org/10.5539/jgg.v4n1p18)
- Safaei M, Omar H, Huat BK, Yousof ZBM, Ghiasi V (2011) Deterministic rainfall induced landslide approaches, advantage and limitation. *EJGE*:1691–1650, <http://www.ejge.com/2011/Ppr11.177/Ppr11.177alr.pdf>
- Schuster RL (1995a) Keynote paper: recent advances in slope stabilization. In: Bell Ed., *Landslides*, Balkema, Rotterdam
- Schuster RL (1995b) Socioeconomic significance of landslides. In: Turner AK, Schuster RL (eds) *Landslides, investigation and mitigation*, transportation research board special report, 247. National Academy Press, WA
- Schuster RL, Fleming RW (1986) Economic losses and fatalities due to landslides. *Bull Am As Eng Geol* 23(1)
- Sidle RC (1984) Relative importance of factors influencing landsliding in coastal Alaska. 21st Annual engineering geology and soils engineering symposium. University of Idaho, Moscow, pp 311–325
- Skempton AW, De Lory FA (1957) Stability of natural slopes in London clay. In: Proceedings 4th international conference on soil mechanics and foundation engineering, vol 2, pp 378–381
- Soeters R, van Westen CJ (1996) Slope instability recognition, analysis and zonation. In: Turner AK, Schuster RL (eds) *Landslides, investigation and mitigation*. Transportation Research Board, National Research Council, special report 247, National Academy Press, Washington, pp 129–177
- Stroia F, Armaş I, Damian R (2005) Earth sliding recently revival in Breaza area on Prahova Valley. In: Proceeding of international symposium on latest natural disasters—new challenges for engineering geology, geotechnics and civil protection, Bulgaria National Group of IAEG, Abstract Book p. 93, CD section 20: 6, Sofia
- Teodorescu A (1984) *Proprietatile rocilor*, ed. Tehnica, Bucharest
- Terzaghi K (1925) *Erdbaumechanik auf Bodenphysikalischer Grundlage*. Franz Deuticke, Wien
- Terzaghi K (1943) *Theoretical soil mechanics*. Wiley, New York
- Thaiyuenwong S, Maireang W (2010) Triggered-rainfall landslide hazard prediction. *Res Dev J* 21(2):43–50
- Travalletti J, Oppikofer T, Delacourt C, Malet JP, Jaboyedoff M (2008) Monitoring landslide displacements during a controlled rain experiment using a long-range terrestrial laser scanning (TLS), the international archives of the photogrammetry, remote sensing and spatial information sciences, vol XXXVII. Part B5. Beijing
- Ulmer M, Molnar P, Purves R (2009) Influence of DEM and soil property uncertainty on an infinite slope stability model. In: *Proceedings of geomorphometry 2009*. Zurich
- US Geological Survey (1997) *US geological survey landslide hazards program five-year plan 1998–2002*. US Government Printing Office, Washington, DC
- UN/ISDR (United Nations International Strategy for Disaster Reduction) (2004) *Living with risk. A global review of disaster reduction initiatives*. 2004 version. United Nations, Geneva, p. 430. http://www.unisdr.org/eng/about_isdr/bd-lwr-2004-eng.htm. Accessed Jan 2012
- van Westen CJ (2000) The modelling of landslide hazards using GIS. *Surv Geophys* 21:241–255. doi:[10.1023/A:1006794127521](https://doi.org/10.1023/A:1006794127521)
- van Westen CJ, and Terlien, M.T.J. (1996) An approach towards deterministic landslide hazard analysis in GIS: a case study from Manizales, Colombia. In: *Earth surface processes and landforms: the journal of the British geomorphological research group*, 9, pp 853–868
- van Westen CJ, Rengers N, Terlien MT, Soeters R (1997) Prediction of the occurrence of slope instability phenomena through GIS-based hazard zonation. *Geol Rundsch* 86(2):404–414. doi:[10.1007/s005310050149](https://doi.org/10.1007/s005310050149)
- van Westen CJ, van Asch TWJ, Soeters R (2006) Landslide hazard and risk zonation—why is it still so difficult? *Bull Eng Geol Env* 65:167–184. doi:[10.1007/s10064-005-0023-0](https://doi.org/10.1007/s10064-005-0023-0)

- van Westen CJ, Castellanos E, Kuriakose SL (2008) Spatial data for landslide susceptibility, hazard, and vulnerability assessment: an overview. *Eng Geol* 102(3–4):112–131. doi:[10.1016/j.enggeo.2008.03.010](https://doi.org/10.1016/j.enggeo.2008.03.010)
- Varnes DJ (1978) Slope movement types and processes. In: Special report 176: landslides: analysis and control, Transportation Research Board, Washington, DC
- Vartolomei F, Armaş I (2010) The intensification of the anthropic pressure through the expansion of the constructed area in the subcarpathian sector of the Prahova Valley/Romania (1800–2008). *Forum Geogr* 9:125–132
- WP/WLI (International Geotechnical Societies UNESCO Working Party on World Landslide Inventory) (1990) A suggested method for reporting a landslide. *Bull Int Assoc Eng Geol* 41:5–12
- WP/WLI (International Geotechnical Societies UNESCO Working Party on World Landslide Inventory) (1993) A suggested method for describing the activity of a landslide. *Bull Int Assoc Eng Geol* 47:53–57
- Wu W, Sidle RC (1995) A distributed slope stability model for steep forested basins. *Water Resour Res* 31(8):2097–2110. doi:[10.1029/95WR01136](https://doi.org/10.1029/95WR01136)
- Yong H, Hiromasa H, Kazuo S, Kyoji S, Akira S, Hiroshi F, Gonghui W (2005) The influence of intense rainfall on the activity of large-scale crystalline schist landslides in Shikoku Island, Japan. *Landslides* 2(2):97–105. doi:[10.1007/s10346-004-0043-z](https://doi.org/10.1007/s10346-004-0043-z)